Developmental Biology 392 (2014) 108–116

Contents lists available at ScienceDirect

Developmental Biology

journal homepage: www.elsevier.com/locate/developmentalbiology

Phosphorylation of CDK2 at threonine 160 regulates meiotic pachytene and diplotene progression in mice

Wenjing Liu [a,b], Lu Wang [a], Weidong Zhao [c], Gendi Song [c], Rener Xu [d], Guishuan Wang [a], Fei Wang [a], Wenqing Li [a], Jie Lian [a], Hui Tian [a], Xiaorong Wang [a], Fei Sun [a,*]

[a] Hefei National Laboratory for Physical Sciences at Microscale and School of Life Sciences, University of Science and Technology of China, Hefei, Anhui 230026, China
[b] College of Life Science and Technology, Southwest University of Science and Technology, Mianyang, Sichuan 621000, China
[c] Engineering College of Animal Husbandry and Veterinary Science, Henan Agricultural University, Zhengzhou, Henan 450002, China
[d] Institute of Developmental Biology and Molecular Medicine and School of Life Science, Fudan University, Shanghai 200433, China

ARTICLE INFO

Article history:
Received 26 December 2013
Received in revised form
31 March 2014
Accepted 26 April 2014
Available online 4 May 2014

Keywords:
p39^{cdk2}/p-CDK2
SUN1
Meiosis
Telomere clustering
Synapsis
Recombination
Mouse
MLH1

ABSTRACT

Telomere clustering is a widespread phenomenon among eukaryotes. However, the molecular mechanisms that regulate formation of telomere clustering in mammalian meiotic prophase I, are still largely unknown. Here, we show that CDK2, especially p39^{cdk2}, as a potential meiosis-specific connector interaction with SUN1 mediates formation of telomere clustering during mouse meiosis. The transition from CDK2 to p-CDK2 also regulates the progression from homologous recombination to desynapsis by interacting with MLH1. In addition, disappearance of CDK2 on the telomeres and of p-CDK2 on recombination sites, were observed in *Sun1*$^{-/-}$ mice and in pachytene-arrested hybrid sterile mice (pwk × C57BL/6 F1), respectively. These results suggest that transition from CDK2 to p-CDK2 plays a critical role for regulating meiosis progression.

Introduction

Meiosis is a critical stage of gametogenesis during which alignment and synapsis of chromosomal pairs occur, allowing for the recombination between maternal and paternal genomes. A prominent feature of meiotic chromosome behavior is the anchoring of chromosome segments, usually telomeres, to the nuclear envelope (NE). The anchored segments interact with SUN and KASH-domain proteins, and cytoskeleton elements, thereby driving chromosome movements and, often highly polarized clustering of chromosome ends into a "bouquet" like structure (also referred to as telomere clustering) (Ding et al., 2007; Hiraoka and Dernburg, 2009; Scherthan, 2007). Telomere clustering thus facilitates homologous chromosome pairing and recombination initiation during meiotic prophase I (MI) (Ding et al., 2007; Harper et al., 2004; Scherthan, 2001). Although the roles of telomere clustering in budding and fission yeast have been extensively studied (Chikashige et al., 2006; Conrad et al., 1997; Cooke and Saunders, 2002; Liebe et al., 2006; Scherthan, 2006; Scherthan et al., 2000, 2011; Trelles-Sticken et al., 2000), these roles in mammals are poorly understood.

During meiosis in fission yeast, telomere clustering involves a common cast of players: NE proteins containing SUN or KASH domains such as SUN1 and SUN2 (Malone et al., 1999; Starr and Han, 2002; Starr et al., 2001), meiosis-specific connector proteins, and cytoskeletal proteins (Hiraoka and Dernburg, 2009). The loss of SUN1 in mice prevents meiotic telomere attachment, homologous pairing and synapsis (Ding et al., 2007; Schmitt et al., 2007), indicating that SUN1–telomere interactions are essential for telomere dynamic movements and then meiotic progression. The meiosis-specific connectors between telomeres and the NE, including Bqt1 and Bqt2 in *S. pombe* (Chikashige et al., 2006), Ndj1 in *S. cerevisiae* (Conrad et al., 1997), and the ZIM/HIM-8 family in *C. elegans* (Phillips and Dernburg, 2006; Phillips et al., 2005), are unique to specific evolutionary lineages (Hiraoka and Dernburg, 2009). However, to our knowledge, the connectors or their roles in SUN1–telomere interactions are still unidentified in mammals.

The progression of the distinct phases in MI is orchestrated by periodic synthesis and degradation of cyclins, the activity of cyclin dependent kinases (CDKs), the correct formation of the synaptonemal complex (SC), and the proper functioning of DNA repair machinery during recombination (Marcon et al., 2008; Ward et al.,

* Corresponding author. Fax: +86 551 63602703.
E-mail address: feisun@ustc.edu.cn (F. Sun).

http://dx.doi.org/10.1016/j.ydbio.2014.04.018
0012-1606/

2007). Several CDKs have been implicated in the progression of meiosis, including CDK1, CDK2, CDK4, and CDK6 (Cohen et al., 2006). For example, CDK2 localizes to telomeres, asynapsed axes of sex chromosomes and co-localizes with MLH1 at sites of reciprocal recombination (Ashley et al., 2001; Viera et al., 2009). In addition, *Cdk2*$^{-/-}$ mice display defects in telomere-NE associations and pachytene arrest with abnormal synapsis and recombination (Viera et al., 2009). These studies lead us to ask whether CDK2-mediated association with NE involves in the formation of telomere clustering. In this study, we validated the roles of CDK2 in telomere clustering during mammalian meiosis.

Materials and methods

Animals

A mouse line carrying a targeted disruption of the *Sun1* gene was maintained in a *C57BL/6J* background by mating heterozygous (*Sun1*$^{+/-}$) males and females (Ding et al., 2007). Genotyping was performed by PCR analysis of genomic DNA as described previously (Supplementary Table 1) (Ding et al., 2007).

CD1 (*ICR*) mice, *C57BL/6* mice and hybrid sterile male mice (*pwk* × *C57BL/6* F1) (Song et al., 2011) were respectively obtained from the Animal Center of University of Science and Technology of China (USTC) and Henan Agricultural University. They were housed under a 14-h light, 10-h dark cycle at room temperature (22 °C). Mice were provided food and water ad libitum. This study received ethical approval from the institutional review boards of the USTC.

Antibodies

Antisera were generated in two rabbits against the synthetic polypeptide, CSYLEVAASQGG, corresponding to the biologically active specific peptide of mouse p39^{cdk2}. Rabbit polyclonal p39^{cdk2} antibody was produced at Abgent Biotechnology Company (Suzhou, China). Western blotting analysis revealed that in mouse testes, the p39^{cdk2} antibody detected one positive protein band whose estimated molecular masses were 39 kDa (upper panel, Fig. S1A).

Histological analysis, immunohistochemistry and immunofluorescence analysis

Mice at indicated ages were euthanized by cervical dislocation. Whole testes were dissected out, fixed in Bouin's solution or 4% paraformaldehyde overnight, embedded in paraffin wax and sectioned at 4 μm. The sections were then used for histological evaluation, immunohistochemical detection of protein expression and TUNEL assay as described previously (Beyret and Lin, 2011; Lian et al., 2010). Specially, for histological evaluation, sections were fixed with Bouin's solution, and stained with hematoxylin and eosin using standard techniques. For immunoflourescent detection of proteins on cryosections, 8–10 μm cryosections were used as described (Beyret and Lin, 2011).

For preparation of nuclear spreads, the drying-down technique (Peters et al., 1997) was used in *C57BL/6* mice, *Sun1*$^{+/+}$ and *Sun1*$^{-/-}$ mice, and in hybrid sterile male mice (*pwk* × *C57BL/6* F1) by double or consecutive immunolabeling with CDK2/MLH1/SYCP3, p-CDK2/MLH1/SYCP3, CDK2/SUN1/SYCP3 and p-CDK2/SUN1/SYCP3. Squash preparations were performed as described previously (Page et al., 1998). For double immunolabeling, an appropriate mixture of secondary antibodies was used. Finally, slides were rinsed in PBS, stained for 3 min with DAPI (49, 6-diamidino-2-phenylindole) (Sigma), rinsed in PBS for a short time and mounted in Vectashield (Vector). The edges of the coverslips were sealed with rubber cement (Elmer's Products, Inc.). Labeled cells were observed and photographed with a Nikon ECLIPSE 80j microscope using the appropriate single or double fluorescence.

To detect proteins, we used the following antibodies and dilutions: mouse anti-CDK2 (Abcam), 1:100 to 1:200; rabbit anti-CDK2 (Abcam), 1:200 to 1:400; rabbit anti-p-CDK2 (Abcam), 1:100 to 1:200; rabbit anti-MLH1 (Oncogene), 1:100 to 1:200; rabbit anti-SYCP3 (Abcam), 1:500; mouse anti-SYCP3 (Abcam), 1:500; rabbit anti-SYCP1 (Abcam), 1:200; mouse anti-SYCP1 (gift from Howard J. Cooke), 1:200; human CREST antiserum (Immunovision, Inc), 1:3000; rabbit anti-γH2AX (Abcam), 1:1000; rabbit anti-SUMO1 (Abcam), 1:1000; rabbit anti-HORMAD1 and rabbit anti-HORMAD2 (gift from Christer Ho og), 1:10,000; and rabbit anti-SUN1 (gift from Rener Xu), 1:500. Signals were visualized by secondary antibodies as follows: donkey anti-mouse Alexa Fluor 488 (Molecular Probes), 1:1000; donkey anti-mouse Alexa Fluor 555 (Molecular Probes), 1:1000; donkey anti-rabbit Alexa Fluor 488 (Molecular Probes), 1:200; donkey anti-rabbit Alexa Fluor 555 (Molecular Probes), 1:200.

Transfection and immunoprecipitation in vitro

Total RNA was isolated from each tissue using TRIzol reagent (Invitrogen). Equal amounts of the RNA were reverse transcribed into cDNA using oligo-dT primers and SuperScript II reverse transcriptase (Invitrogen). The full-length open reading frames encoding *Cdk2*, *Mlh1*, and *Sun1* were amplified from mouse testis cDNA using primer pairs (Supplementary Table 2). PCR products were subcloned into pCRII (TAKARA), sequenced, and finally cloned into the eukaryotic expression vector p3XFLAG-myc-CMV™-24 (Sigma) and pEGFP-C1 (BD Biosciences Clontech) at the EcoRI and SalI sites. The HEK293T cell line (gift from Mian Wu) was cultured and transfected with the plasmids using Lipofectamine 2000 (Invitrogen) according to the manufacturer's instructions. The cells were fixed in 4% paraformaldehyde (PFA) and permeabilized with 0.1% Triton X-100 for immunostaining. The cells were extracted in IP buffer containing 25 mM Tris–HCl (pH 7.5), 150 mM NaCl, 5 mM EDTA, 1% Triton X-100, 0.5% Na-deoxycholate, 0.1% SDS, and protease inhibitors for immunoprecipitation in vitro, as described next. Cell extracts were pre-cleared with protein A-conjugated Dynabeads (Invitrogen) and incubated with the anti-FLAG or anti-GFP antibody bound to protein A-conjugated Dynabeads (Invitrogen) overnight at 4 °C. Immunoprecipitated pellets were washed four times in NP-40 free IP buffer, eluted in protein sample buffer, and subjected to Western blotting.

GST pull-down

The cDNAs encoding full-length *Cdk2*, *Sun1* in mice were recovered by EcoRI and SalI digestion and subcloned into the glutathione S-transferase (GST) fusion vector pGEX-5X-3 (Pharmacia) and HIS.Tag fusion vector pET-21a-d (Novagen) by standard procedures. Recombinant proteins were detected and purified as described previously (Berruti, 2000). Fusion proteins, immobilized on glutathione-Sepharose, were eluted by incubation with 50 mM Tris–HCl, 150 mM NaCl, 20 mM glutathione (pH 7.5) for 30 min at 4 °C, dialyzed overnight against 50 mM Tris–HCl, 1 mM dithiothreitol (pH 7.5), and stored at 4 °C. The purity of the His- or GST-fused proteins was judged by SDS-PAGE and Coomassie brilliant blue staining (Sigma). Protein concentrations were assessed by comparison with bovine serum albumin standards using the Bio-Rad DC protein assay.

For GST pull-down experiments, freshly prepared cell lysates from 20d and adult *ICR* mice testes were incubated with purified GST-SUN1 or GST alone for 2 h at 4 °C, followed by 1 h of

incubation with glutathione-Sepharose beads (GE healthcare). The complexed beads were recovered by centrifugation; washed four times with TNE buffer [10 mM Tris–HCl (pH 7.5), 150 mM NaCl, 1 mM EDTA, 1% Nonidet P-40, 10 mg (each) of leupeptin and aprotinin per milliliter]; and solubilized in SDS-PAGE sample buffer to be first resolved by SDS-PAGE and then analyzed by Western immunoblotting. The specific proteins followed by identification with MALDI-TOF-TOF mass spectrometry (UltrafleXtreme) in USTC (data not shown).

Western blotting

To detect the expression of CDK2 and p-CDK2 at days 0, 5, 10, 15, 20, 35 and 60 of neonatal life in *ICR* mice, testicular tissues were extracted in a RIPA buffer [50 mM Tris–HCl (pH7.5), 150 mM NaCl, 1 mM EDTA, 1% Triton X-100, 1% Na-deoxycholate, 1% SDS, and protease inhibitors]. The primary and secondary antibodies used for all immunoblotting and other experiments are listed in Supplementary Table 3. Signals were detected with Hybond enhanced chemiluminescence (ECL) Nitrocellulose membranes (Amersham Biosciences, Freiburg, Germany), immunoblotted with antibodies, and visualized by ECL (Kodak, Rochester, NY, USA).

Evaluation of specificity of p-CDK2 antibody

To detect the specificity of p-CDK2 antibody, point-mutant version, namely Flag-p39CDK2 (m), in which the ACU codon (Thr160) was mutated to AAU, was transfected in vitro (Fig. S4, A and B). Specificity of p-CDK2 antibody from Santa Cruz company (Fig. S4C, I) and Abcam company (Fig. S4C, II and III) has no difference by spread technology.

Results

$p39^{cdk2}$ preferentially interacts with SUN1

In *Cdk2*$^{-/-}$ spermatocytes, some telomeres do not attach to the NE, indicating an important role for CDK2 in meiosis (Viera et al., 2009). Two isoforms of CDK2 ($p39^{cdk2}$ and $p33^{cdk2}$) were identified to be expressed in given organs (Berthet et al., 2003). Phosphorylation of CDK2 on threonine 160 is essential for its kinase activity (Ukomadu and Dutta, 2003). Here, the expression patterns of CDK2 and phosphorylated CDK2 (p-CDK2, Thr160) were first examined in the testis of *ICR* mice at days 0, 5, 10, 15, 20, 35 and 60 of neonatal life, and in different tissues of adult mice (Fig. 1A and B). $p39^{cdk2}$ and $p33^{cdk2}$ were detected with anti-p-CDK2 and anti-CDK2 antibodies in the testis, spleen, and thymus (Fig. 1B). To further ascertain the role of $p39^{cdk2}$, we generated the rabbit polyclonal $p39^{cdk2}$ antibody (Fig. S1A). $p39^{cdk2}$ was also expressed in the testis and thymus (lower panel, Fig. 1B). In general, the expression levels of $p33^{cdk2}$ had no obvious change from 0d to 35d, but it decreased at 60d (Fig. 1A); while both the expression levels of $p39^{cdk2}$, $p39^{p\text{-}cdk2}$ (Fig. 1A) and the band intensity ratio of $p39^{cdk2}/p33^{cdk2}$ (Fig. S1B) were gradually increased at different days of neonatal life in mouse testes. These results indicate that $p39^{cdk2}$ may compete with $p33^{cdk2}$ during meiotic progression. Noguchi et al. (1993) also observed that $p39^{cdk2}$ functioned as a negative regulator at G1/S transition by competing with $p33^{cdk2}$ in BHK21 cell mitosis.

GST pull-down assays verified the interaction between CDK2 and the N-terminus of SUN1 (GST-SUN1NTD) from testes lysates (Fig. 1C). In addition, GST-SUN1NTD bound to $p39^{cdk2}$ stronger than $p33^{cdk2}$ in 20d (Fig. 1C) and 60d (Fig. S1C) mouse testes. This interaction was corroborated by co-immunoprecipitation (Co-IP) experiments using lysates from HEK293T cells co-expressing recombinant CDK2 and SUN1 proteins. For example, GST-SUN1NTD was able to interact with His-mCDK2-p39 in vitro (Fig. S1D); FLAG-$p39^{cdk2}$ strongly bound to GFP-SUN1 and FLAG-$p33^{cdk2}$ weakly bound to GFP-SUN1 in vitro (Fig. 1D). Immunoprecipitation of testis lysate with the $p39^{cdk2}$ specific antibody also demonstrated that the $p39^{cdk2}$ could pull down SUN1 (Fig. 1E). The SUN1–$p39^{cdk2}$ interaction was further characterized in testis preparations from wild-type and *Sun1*$^{-/-}$ mice (Fig. 1F and G). In the testis of wild-type mice, SUN1 and $p39^{cdk2}$ co-localized from leptotene to diplotene and disappeared at diakinesis during MI (left panel, Figs. 1F; S1E showing SUN1only), but p-CDK2 began to co-localize with SUN1 from mid-pachytene to diplotene (right panel, Fig. 1F). Notably, $p39^{cdk2}$ was not loaded on the meiotic telomeres in *Sun1*$^{-/-}$ mice, and dispersed in the nucleus during zygotene-like stages (Fig. 1G). The ring chromosomes were also detected in *Sun1*$^{-/-}$ mice (Fig. 1G), which was similar to those observed in testis preparations from *Cdk2*$^{-/-}$ mice (Viera et al., 2009). Indeed, $p39^{cdk2}$ was localized on chromosome telomeres (Fig. 1H). In addition, $p39^{cdk2}$ expression was decreased in *Sun1*$^{-/-}$ mice (Fig. S2B).Together with these results, $p39^{cdk2}$ was expressed in the testis in patterns that suggested unique, cell-specific functions for meiosis.

Dynamic distributions of $p39^{cdk2}$ and p-CDK2 on the chromosomes during MI of normal male mice

Next, the distribution of $p39^{cdk2}$ and p-CDK2 on the chromosomes were studied in detail during mouse meiosis by using the SC spread (Peters et al., 1997) and squash techniques (Page et al., 1998). Three localization patterns of $p39^{cdk2}$ in meiotic prophase nuclei were identified: (1) at telomeres (Figs. 1F; 2A and C), (2) at one to two (rarely three) interstitial sites per bivalent beginning near the early- to mid-pachytene transition (Figs. 2A and 3) on the asynapsed axes of sex chromosomes during pachytene and diplotene (Fig. 2A). The telomeric $p39^{cdk2}$ signals began to form during the leptotene stage, became prominent throughout zygotene and pachytene, and then began to disappear during late diplotene. The $p39^{cdk2}$ interstitial foci disappeared from the autosomal SCs by late pachytene (Fig. 2A). As for p-CDK2, there were three localization patterns in meiotic prophase nuclei (Fig. 2B and D): (1) at one to two (rarely three) interstitial sites per bivalent beginning near the mid to late-pachytene transition, (2) at telomeres during mid-pachytene and diakinesis, and (3) on the asynapsed axes of sex chromosomes, the sex body and the dense body (arrowhead). Notably, p-CDK2 had no signals at telomeres from leptotene to early pachytene (Fig. 2B and D). These results indicated that the phosphorylation sites of $p39^{cdk2}$ may be blocked at telomeres from leptotene to pachytene, or were only activated with its partner (s) during mid-pachytene and diakinesis.

Distributions of $p39^{cdk2}$ and p-CDK2 on the chromosomes during MI of hybrid sterile male mice

The distribution of p-CDK2 on the chromosomes was also studied in *pwk* × *C57BL/6* F1 (PCF1) male mice. The phenotype of PCF1 mice was confirmed by staining sections of the testes and epididymides with hematoxylin and eosin (HE). As shown in Fig. 3A, most spermatocytes of PCF1 male mice arrested in pachytene (Fig. 3A, I and II); a few of seminiferous tubules contained only Sertoli cells, and there was no sperm in their epididymides (Fig. 3A, III and IV). Germ cell apoptosis was analyzed in the testes of C57 and PCF1 male mice (Fig. 3B) by immunohistochemical staining using in situ terminal deoxynucleotidyl transferase dUTP nick end labeling (TUNEL). The results showed that positive TUNEL staining was detected predominantly in spermatogonia and spermatocytes, but the apoptosis rate was

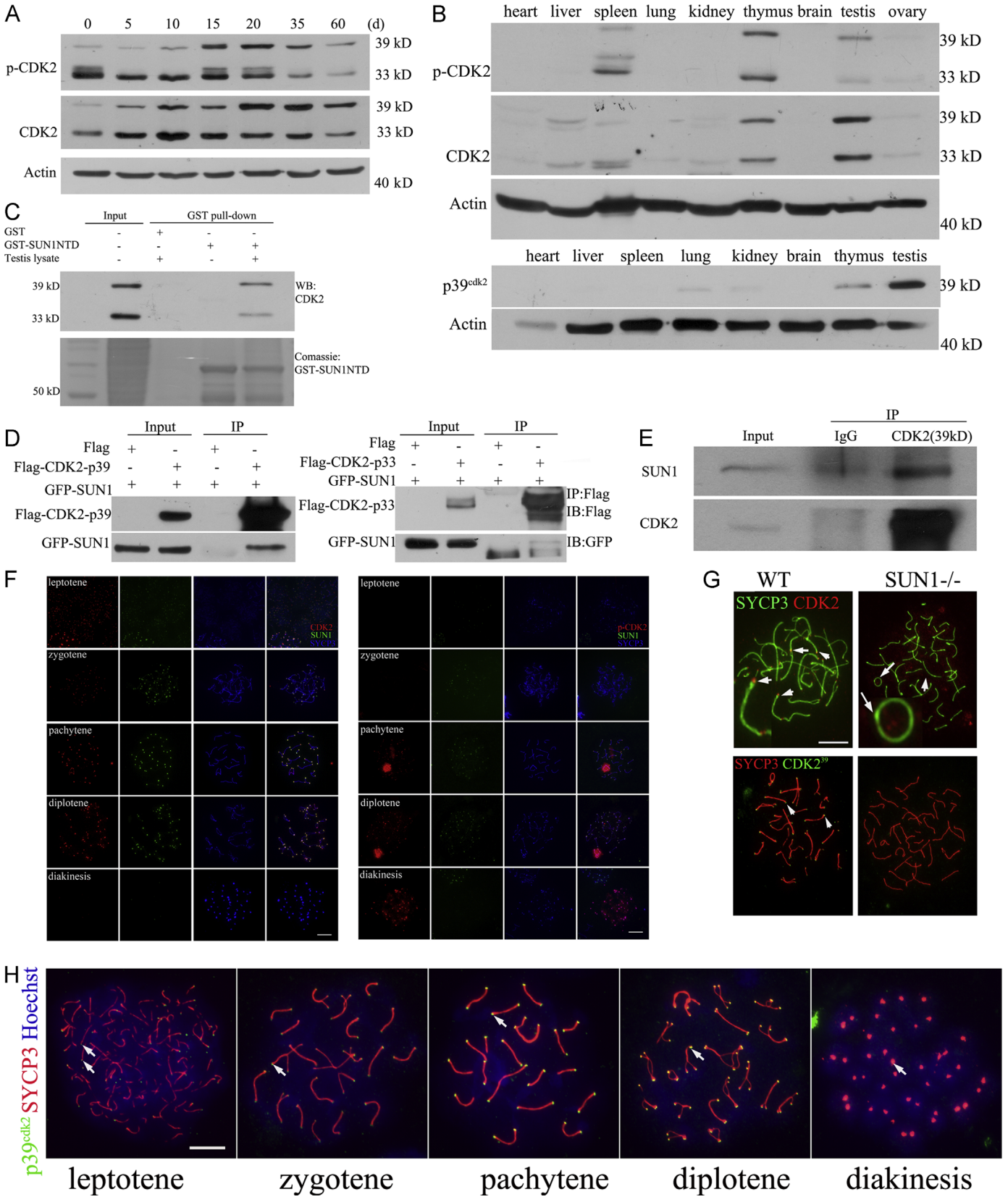

Fig. 1. CDK2 interaction and co-localization with SUN1. (A) Expression patterns of CDK2 and p-CDK2 at different days of neonatal life. The upper bands represent $p39^{cdk2}$ and the lower bands represent $p33^{cdk2}$ in the p-CDK2 and CDK2 rows. (B) Expression patterns of CDK2/p-CDK2 (upper panel) and $p39^{cdk2}$ (lower panel) in different tissues. (C) A GST-SUN1 N-terminal domain (NTD) pull-downs CDK2 from 20d *ICR* mouse testis tissues. GST-SUN1NTD strongly binds to $p39^{cdk2}$, and weakly binds to $p33^{cdk2}$. (D) FLAG-CDK2-p39 (left panel) and FLAG-CDK2-p33 (right panel) immunoprecipitated GFP-SUN1. FLAG-CDK2-p39 interacts with GFP-SUN1 stronger than FLAG-CDK2-p33. (E) Co-immunoprecipitation (IP) using antibodies to $p39^{cdk2}$ followed by Western blotting using an antibody to SUN1. (F) Immunofluorescence co-localization of CDK2 and SUN1. In nuclear spread experiments, CDK2 (red) and SUN1 (green) co-localize at the telomeres of chromosomes (blue) from leptotene to diplotene during MI in normal mice (left panel). p-CDK2 (red) and SUN1 (green) co-localize at the telomeres of chromosomes (blue) from mid-pachytene to late diplotene during MI (right panel). $n=30$ ($n=$number of chromosome spreads per staining). (G) Localization of CDK2 on the telomeres of chromosomes in wild-type and $Sun1^{-/-}$ mice. $n=100$. (H) Localization of $p39^{cdk2}$ (green, arrow) on the telomeres of chromosomes (red) during meiosis. $n=30$. Scale bars: 10 μm.

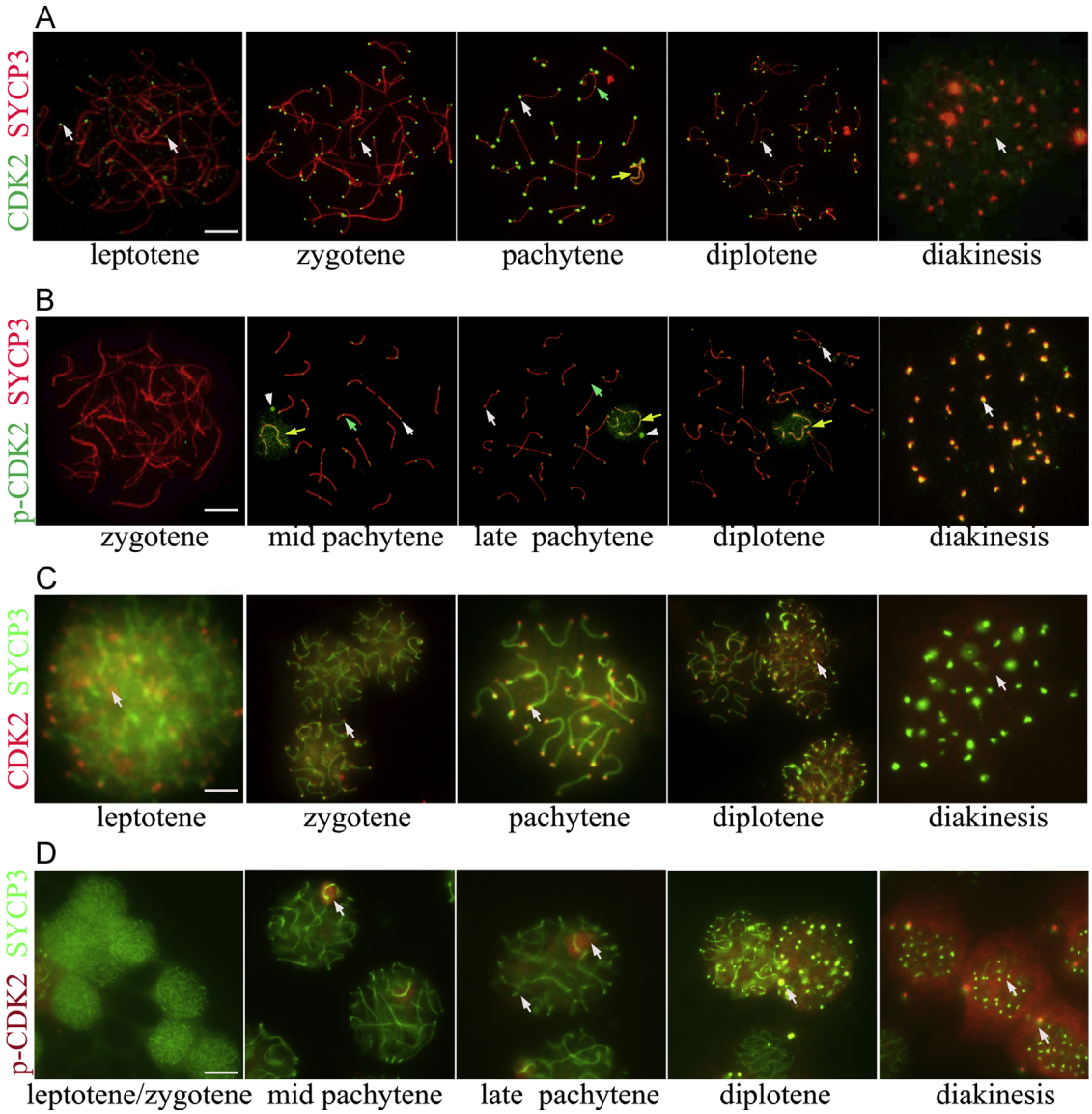

Fig. 2. Dynamic distributions of CDK2 and p-CDK2 on chromosomes in normal mouse testes. (A and B) Dynamic localization of CDK2 and p-CDK2 in nuclear spreads from leptotene to diakinesis during MI. SYCP3 (red) and CDK2 (green) (A), and SYCP3 (red) and p-CDK2 (green) (B) were labeled, respectively. (A) There are three localization patterns of CDK2 in meiotic prophase nuclei: (1) at telomeres from leptotene to diplotene (white arrow), (2) at one to two interstitial sites per bivalent beginning near the early- to mid-pachytene transition (green arrow), and (3) on the asynapsed axes of sex chromosomes during pachytene and diplotene (yellow arrow). CDK2 disperses in the nuclear at diakinesis (white arrow). (B) p-CDK2 has three localization patterns in meiotic prophase nuclei: (1) at one to two interstitial sites per bivalent beginning near the mid to late-pachytene transition (green arrow), (2) at telomeres from mid-pachytene to diakinesis (white arrow), (3) on the asynapsed axes of sex chromosomes (yellow arrow) and sex bodies (white arrowhead) during pachytene and early diplotene. $n=50$ ($n=$number of chromosome spreads per staining). (C and D) Dynamic distributions of CDK2 and p-CDK2 by squash from leptotene to diakinesis during MI. SYCP3 (green) and CDK2 (red, white arrow) (C), and SYCP3 (green) and p-CDK2 (red, white arrow) (D) were labeled, respectively. Telomeric CDK2 is present during the leptotene stage, becomes prominent throughout zygotene and pachytene, and then begins to disappear during the end of diakinesis (white arrow). p-CDK2 is present at telomeres during the late pachytene and diakinesis (white arrow). $n=30$ ($n=$number of chromosome squash per staining). Scale bars: 10 μm.

not significantly different between the two groups (Fig. 3C). The relative testis weight of PCF1 male mice (3.11 ± 0.15) was significantly lower than that of control mice (5.89 ± 0.27, $P < 0.001$) (Fig. 3D).

The meiotic abnormalities in PCF1 male mice were further investigated by analysis of the distributions of several meiotic proteins, such as SYCPs, DSB, and recombination-related proteins (e.g., MLH1 and CDK2) (Figs. 3E; S3). Compared with control mice, two sex body-like structures (labeled by γH2AX (DSB marker), red), absence of SYCP1 at axis of SCs and unpaired regions of SCs (labeled by HORMAD1 and HORMAD2) were detected in PCF1 male mice. These results showed that the spermatocytes from PCF1 mice had incomplete synapsis and pachytene arrest with many unsynapsed autosomal segments. Interestingly, the CDK2 and p-CDK2 located at sites of reciprocal recombination in control mice, but p-CDK2 disappeared at the same foci in PCF1 male mice, and it was intensively distributed in unpaired autosomal regions during the pachytene stage (Fig. 3E and F). Meanwhile, p-CDK2 depleted or disappeared from sex bodies in PCF1 male mice (Fig. 3F).

p-CDK2 associates with MLH1 to regulate meiotic progression

Since CDK2 and p-CDK2 also located at sites of reciprocal recombination, we next determined whether CDK2 activation was involved in the formation of recombination nodules. Consecutive immunolabeling for SYCP3 and CDK2/p-CDK2 and then MLH1 showed that CDK2 and p-CDK2 had similar interstitial

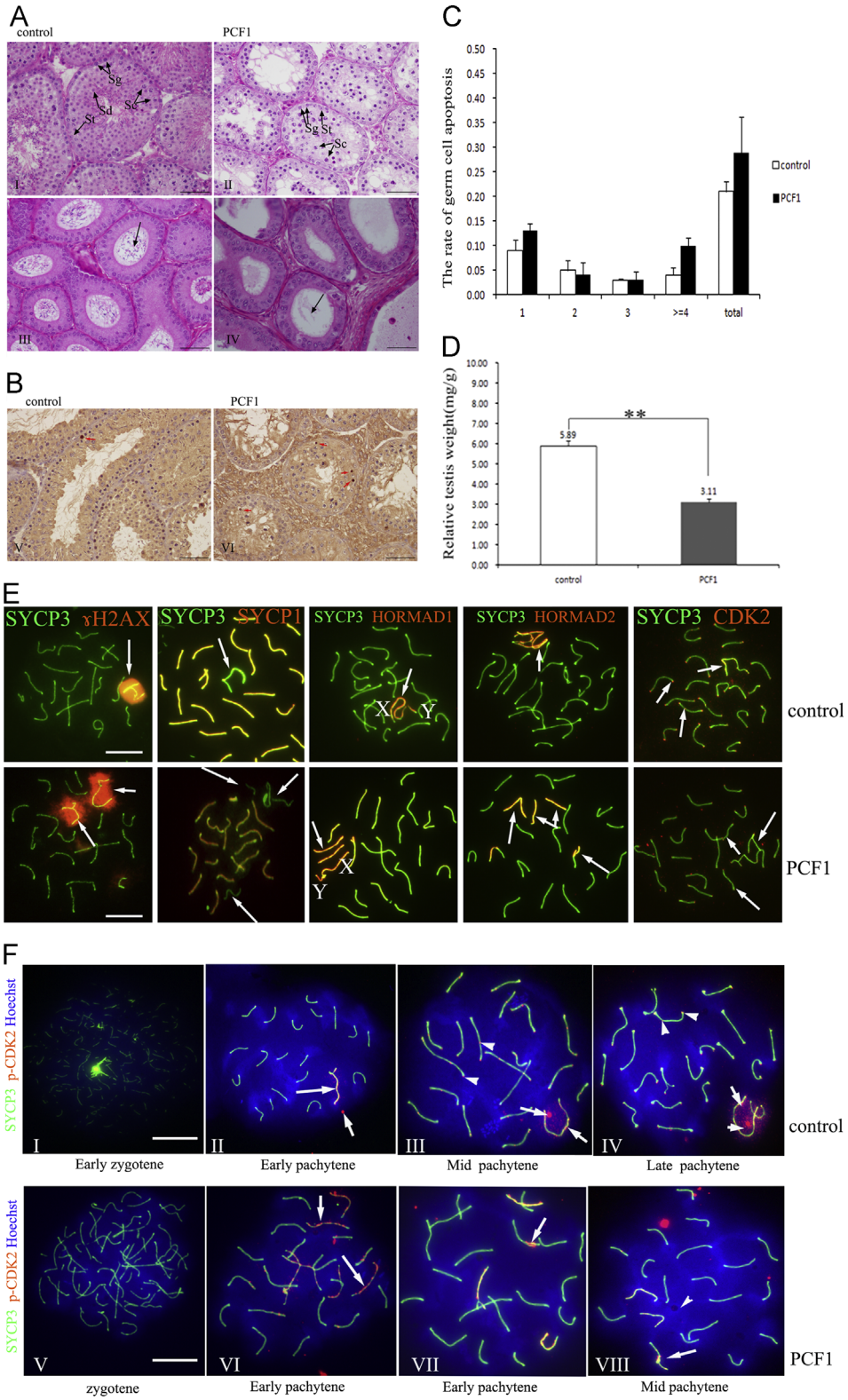

Fig. 3. Distributions of p-CDK2 on chromosomes in hybrid sterile male mice (PCF1). (A) Sections of HE-stained testes and epididymides in control (I and III) and PCF1 male mice (II and IV). The seminiferous tubules of PCF1 male mice contained pachytene-arrested spermatocytes (II, arrow). Sperm is present in the epididymides in control mice (III, arrow), but not in PCF1 male mice (IV, arrow). (B) TUNEL for detecting germ cell apoptosis in control (left panel) and PCF1 mice (right panel). (C) The rate of testicular germ cell apoptosis (TUNEL-positive seminiferous tubules/total seminiferous tubules). (D) Relative testis weights of control and PCF1 mice. (E) The distributions of SC, DSBs and recombination-related proteins on chromosomes in control (upper row) and PCF1 mice (lower row). Two sex body-like structures (γH2AX, red; SYCP3, green) are present at pachytene-arrest stages (arrow). SYCP1 unloads on SYCP3 (arrow). $n=30$ ($n=$number of chromosome spreads per staining). (F) Distributions of p-CDK2 on chromosomes in control and PCF1 mice. $n=30$. Abbreviation: PCF1, *pwk* × *C57BL/6* F1; St, Sertoli cells; Sg, spermatogonia; Sc, primary spermatocyte; and Sd, round spermatids. Scale bars: A and B, 50μm; E and F, 10 μm.

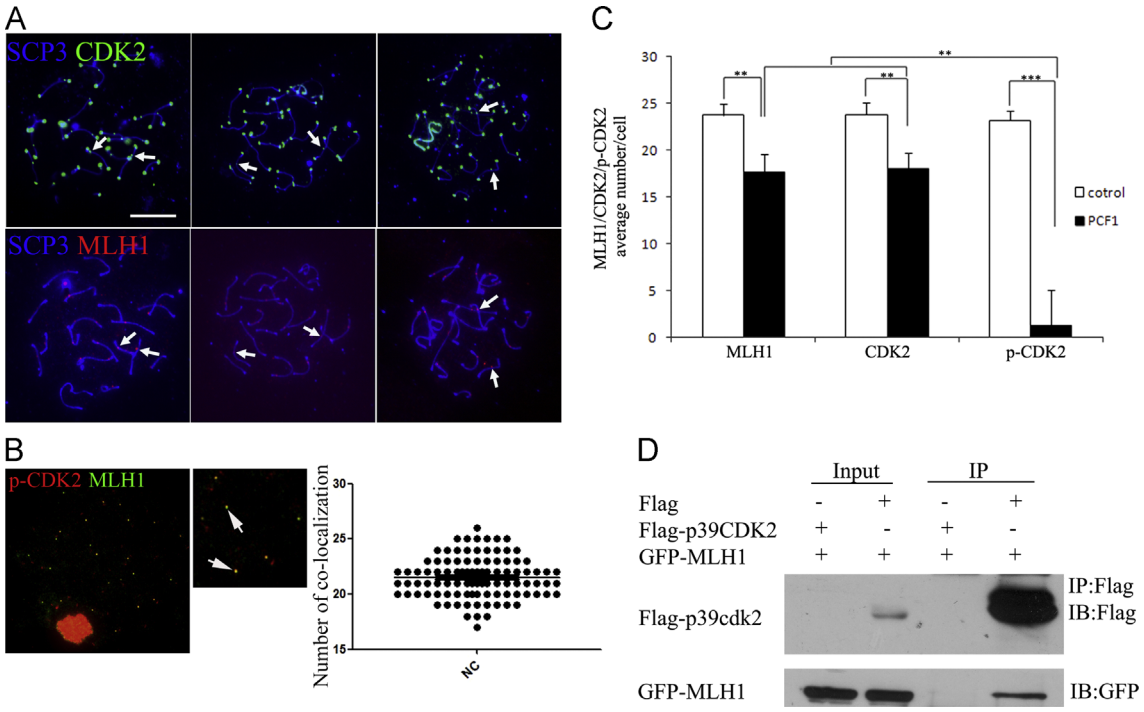

Fig. 4. Co-localization of $p39^{cdk2}$/ p-CDK2 and MLH1 during pachytene. (A, B) CDK2 (green)/MLH1 (red) and p-CDK2 (red) /MLH1 (green) were labeled, respectively, by consecutive labeling experiments in control mice. SYCP3 was stained in blue. CDK2 signals accumulated along the asynapsed axes of sex chromosomes during pachytene. In A, $n=50$ (n=number of chromosome spreads per staining). In B, $n=100$. (C)The average number of interstitial CDK2 or p-CDK2 foci co-localized with MLH1 in the spermatocyte nuclei of control and PCF1 mice. (D) Co-immunoprecipitation of MLH1 and $p39^{cdk2}$. Scale bars: 10 μm.

localization with MLH1 (Fig. 4A and B). In addition, the average number of co-localization of MLH1 and CDK2 foci in PCF1male mice (17.3 ± 1.2) (Fig. S3) was significantly lower than that of C57 mice (23.2 ± 1.3, $P < 0.01$) (Fig. 4C). However, compared with control mice (22.7 ± 1.3), MLH1/p-CDK2 signals only co-localized to a few foci within each nucleus (3.1 ± 1.7, $P < 0.001$) in PCF1 mice (Fig. 4C). Co-IP assays also verified the association between $p39^{cdk2}$ and MLH1 in vitro (Fig. 4D). Indeed, $p39^{cdk2}$ located at the recombination sites during the pachytene stage (Fig. S1A, III). These results indicated that the binding of MLH1 to CDK2 may activate CDK2 during meiotic progression.

Discussion

In this study, we reported that transition from CDK2 to p-CDK2 correlated with formation and dispersion of telomere clustering through interaction with SUN1 during MI in mice. In addition, this transition also correlated with recombination progression through interaction with MLH1. Our results demonstrate, for the first time, that $p39^{cdk2}$ is a potential meiosis-specific connector mediating telomere-NE associations in mice.

Meiotic chromosomes must attach to the NE by their telomeres during MI to facilitate homologous recognition, synapsis and recombination (Scherthan, 2007). The anchoring of telomeres to the NE after DNA replication is completed or redistributed over the nuclear periphery in pre-leptotene (Ding et al., 2007). In leptotene, telomeres of elongated chromosomes have attached randomly over the NE. In pachytene, telomeres of the paired homologs are scattered over the NE. During the progression from pre-leptotene to pachytene, meiosis-specific connectors are needed to mediate the SUN1–telomere interactions (Hiraoka and Dernburg, 2009). Rap1 is required for telomeres to assemble at the NE in fission yeast; however, *Rap1*$^{-/-}$ mice are viable and fertile (Martinez et al., 2010; Sfeir et al., 2010), showing normal assembly of telomeres on the NE (Scherthan et al., 2011). Lack of conservation of Rap1' roles in meiosis between fission yeast and mammals, suggested that mammals have alternative modes for connecting telomeres to SUN proteins (Scherthan et al., 2011). To our current knowledge, these connectors are unidentified in mammals.

In *Cdk2*$^{-/-}$ spermatocytes, some telomeres do not attach to the NE, and easily form the ring chromosomes (Viera et al., 2009). In our study, $p39^{cdk2}$ interacted with SUN1 at telomeres, in addition, CDK2 did not attach to the NE and gave rise to ring chromosomes in the absence of *Sun1* (Fig. 1G). These results suggest that $p39^{cdk2}$ is a potential connector between telomeres and the NE during mammalian meiosis. CDK2 could not be activated from leptotene to early pachytene during MI, rather it could only be activated during late pachytene and diakinesis (Fig. 2B). CDK2/p-CDK2 and MLH1 recombination foci co-localized to the same sites on the SCs in normal mice, but, the co-localization was severely reduced in pachytene-arrested PCF1mice. These results suggest that both MLH1 and CDK2 are components of recombination nodules, and the transition from CDK2 to p-CDK2 regulates mammalian meiotic progression.

The activation of CDK2 is mediated by its protein partners such as cyclins. For example, cyclin A2 preferentially binds the $p33^{cdk2}$ during spermatogenesis (Ravnik and Wolgemuth, 1999), but cyclin A1 preferentially binds the $p39^{cdk2}$ (Sweeney et al., 1996). Cyclin A2 was present only in spermatogonia and preleptotene spermatocytes, while cyclin A1 distributed in nucleus after mid-pachytene and then localized on the telomeres in late diplotene (Ravnik and Wolgemuth, 1999). The location patterns of cyclin A1 on the SCs (Ravnik and Wolgemuth, 1999) coincided with the distribution of p-CDK2 (Fig. 2B). Therefore, we propose that CDK2 is a putative binding partner for cyclin A1 in mid-pachytene during meiosis. However, further studies are required to identify the meiotic partner(s) and variants of CDK2, and to understand other functions of p-CDK2 in meiosis.

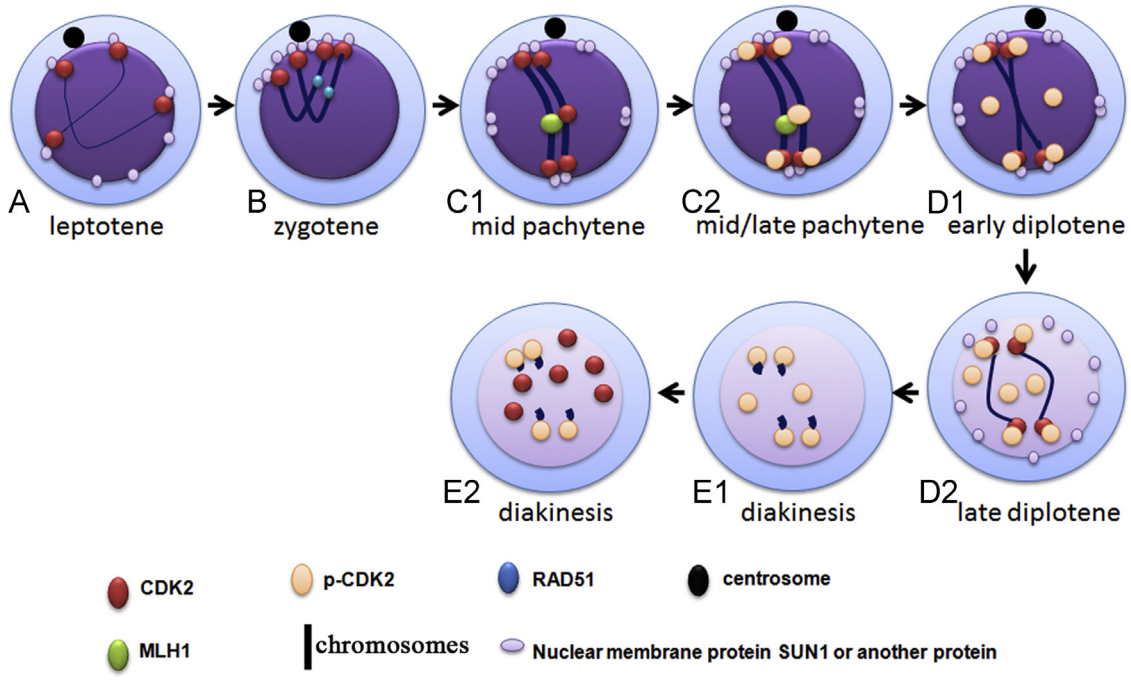

Fig. 5. Model of meiotic regulation by CDK2/p-CDK2/MLH1/SUN1. (A) During leptotene, CDK2 (red), as a part of the telomeres of elongated chromosomes (dark blue), is attached randomly over the NE through interactions with SUN1 (white circle). Telomeres then move to congregate near the centrosome (black) and contribute to homologous recognition. (B) In zygotene, most terminal chromosome fractions are aligned, allowing intensive chromatin interactions (dark blue). RAD51 (blue) loads on chromosomes (dark blue) during this stage. (C1) During mid-pachytene, CDK2 (red) replaces RAD51 foci and binds to the DSB repair foci (recombination foci), thereby recruiting MLH family proteins MLH1 (green) and MLH3 (not shown) to interact with CDK2. (C2) In late pachytene, telomeres of the paired homologs are scattered over the NE. p-CDK2 (pink) co-localizes with MLH1 (green)/SUN1 (white circle) at sites of reciprocal recombination and the telomeres, and then MLH1 detaches from chromosomes by CDK2 activation. (D1) During early diplotene, synapsis of homologous chromosomes (dark blue) begins to dissolve. p-CDK2 (pink) detaches from the reciprocal recombination foci and disperses in the nucleus. (D2) During late diplotene, telomeres of the paired homologs are detached from the NE. CDK2 is activated on the telomeres during this stage. Only p-CDK2 (pink) was present intensively at the telomeres of chromosomes (dark blue). SUN1 was dispersed on the nuclear envelope. (E1, E2) During diakinesis, p-CDK2 (pink) was also present intensively at the telomeres of chromosomes (dark blue), but CDK2 (red) was dispersed in the nucleus. SUN1 disappeared from the NE during this stage.

Based on these results, a unified model for CDK2/p-CDK2/MLH1/SUN1 regulation of meiosis is proposed (Fig. 5). In pre-leptotene, telomeres anchor to the NE after DNA replication (Scherthan, 2001). CDK2 expression begins during this stage (Fig. 2C). During leptotene, CDK2 is a part of the telomeres of elongated chromosomes and is tethered randomly over the NE through interactions with SUN1 (Fig. 5A). Telomeres then move to congregate near the centrosome or its equivalent (mammals, algae, yeast) (Hiraoka and Dernburg, 2009). Alternatively, nuclear rotations could position telomeres near the centrosome where they get captured (Harper et al., 2004; Scherthan, 2001). During these movements, encounters between elongated chromosomes, which probably carry DSBs, such as γH2AX, BRCA1 (not labeled here) loading on chromosomes, contribute to homologous recognition (Ding et al., 2007). During the tightest telomere clustering at the leptotene–zygotene transition, most terminal chromosome fractions are aligned, allowing intensive chromatin interactions. RAD51 loads on chromosomes (Ward et al., 2007). The transit from zygotene to pachytene coincides with the initiation and progression of synapsis and chromosome condensation, which might drive the resolution of the bouquet topology (Fig. 5B) (Ding et al., 2007; Hiraoka and Dernburg, 2009). In pachytene (Fig. 5C1 and C2), three molecular events occur: first, telomeres of the paired homologs are scattered over the NE. Second, initiation of homologous recombination is triggered. CDK2 replaces RAD51 foci and binds to the DSB repair foci (i.e. recombination foci) (Ward et al., 2007), then recruits MLH family proteins including MLH1 and MLH3. MLH1 then detaches from chromosomes by CDK2 activation. Third, silence of X and Y chromosomes results in sex body formation (not labeled here). In diplotene (Fig. 5D1 and D2), homologous chromosomes begin to separate and pull away from each other. p-CDK2 detaches from the reciprocal recombination foci and disperses in the nucleus. Telomeres of the paired homologs are detached from the NE. CDK2 could be activated on the telomeres during this stage (Fig. 5D1 and D2), and SUN1 distribution on the nuclear envelope was dispersed. During diakinesis (Fig. 5E1 and E2), CDK2 was dispersed in the nucleus, and SUN1 disappeared from the NE. Only p-CDK2 was abundant on the telomeres. This model helps in our understanding of the acting mechanisms of CDK2 and p-CDK2 in the meiotic progression.

Acknowledgments

We thank Professor Howard J. Cooke (MRC Human Genetics Unit, Western General Hospital, Edinburgh, UK) for providing rabbit anti-SYCP1 and mouse anti-SYCP1 antibody. We thank Professor Christer Hoog (Department of Cell and Molecular Biology, Karolinska Institutet, Sweden) for providing rabbit anti-HORMAD1/2 antibody. We thank Dr. Mian Wu for the HEK293T cell line, and we also thank Dr. Gang Cai and Dr. Jianye Zang for fusion protein purification in USTC. This work was supported by the following grants (to F.S.): the National Natural Science Foundation of China (81125005), the National Basic Research Program of China (2014CB943100).

Appendix A. Supplementary materials

Supplementary data associated with this article can be found in the online version at http://dx.doi.org/10.1016/j.ydbio.2014.04.018.

References

Ashley, T., Walpita, D., de Rooij, D.G., 2001. Localization of two mammalian cyclin dependent kinases during mammalian meiosis. J. Cell Sci. 114, 685–693.

Berruti, G., 2000. A novel rap1/B-Raf/14-3-3 theta protein complex is formed in vivo during the morphogenetic differentiation of postmeiotic male germ cells. Exp. Cell Res. 257, 172–179.

Berthet, C., Aleem, E., Coppola, V., Tessarollo, L., Kaldis, P., 2003. Cdk2 knockout mice are viable. Curr. Biol. 13, 1775–1785.

Beyret, E., Lin, H., 2011. Pinpointing the expression of piRNAs and function of the PIWI protein subfamily during spermatogenesis in the mouse. Dev. Biol. 355, 215–226.

Chikashige, Y., Tsutsumi, C., Yamane, M., Okamasa, K., Haraguchi, T., Hiraoka, Y., 2006. Meiotic proteins bqt1 and bqt2 tether telomeres to form the bouquet arrangement of chromosomes. Cell 125, 59–69.

Cohen, P.E., Pollack, S.E., Pollard, J.W., 2006. Genetic analysis of chromosome pairing, recombination, and cell cycle control during first meiotic prophase in mammals. Endocr. Rev. 27, 398–426.

Conrad, M.N., Dominguez, A.M., Dresser, M.E., 1997. Ndj1p, a meiotic telomere protein required for normal chromosome synapsis and segregation in yeast. Science 276, 1252–1255.

Cooke, H.J., Saunders, P.T., 2002. Mouse models of male infertility. Nat. Rev. Genet. 3, 790–801.

Ding, X., Xu, R., Yu, J., Xu, T., Zhuang, Y., Han, M., 2007. SUN1 is required for telomere attachment to nuclear envelope and gametogenesis in mice. Dev. Cell. 12, 863–872.

Harper, L., Golubovskaya, I., Cande, W.Z., 2004. A bouquet of chromosomes. J. Cell Sci. 117, 4025–4032.

Hiraoka, Y., Dernburg, A.F., 2009. The SUN rises on meiotic chromosome dynamics. Dev Cell. 17, 598–605.

Lian, J., Tian, H., Liu, L., Zhang, X.S., Li, W.Q., Deng, Y.M., Yao, G.D., Yin, M.M., Sun, F., 2010. Downregulation of microRNA-383 is associated with male infertility and promotes testicular embryonal carcinoma cell proliferation by targeting IRF1. Cell Death Dis. 1, e94.

Liebe, B., Petukhova, G., Barchi, M., Bellani, M., Braselmann, H., Nakano, T., Pandita, T.K., Jasin, M., Fornace, A., Meistrich, M.L., Baarends, W.M., Schimenti, J., de Lange, T., Keeney, S., Camerini-Otero, R.D., Scherthan, H., 2006. Mutations that affect meiosis in male mice influence the dynamics of the mid-preleptotene and bouquet stages. Exp. Cell Res. 312, 3768–3781.

Malone, C.J., Fixsen, W.D., Horvitz, H.R., Han, M., 1999. UNC-84 localizes to the nuclear envelope and is required for nuclear migration and anchoring during *C. elegans* development. Development 126, 3171–3181.

Marcon, E., Babak, T., Chua, G., Hughes, T., Moens, P.B., 2008. miRNA and piRNA localization in the male mammalian meiotic nucleus. Chromosome Res. 16, 243–260.

Martinez, P., Thanasoula, M., Carlos, A.R., Gomez-Lopez, G., Tejera, A.M., Schoeftner, S., Dominguez, O., Pisano, D.G., Tarsounas, M., Blasco, M.A., 2010. Mammalian Rap1 controls telomere function and gene expression through binding to telomeric and extratelomeric sites. Nat. Cell Biol. 12, 768–780.

Noguchi, E., Sekiguchi, T., Yamashita, K., Nishimoto, T., 1993. Molecular cloning and identification of two types of hamster cyclin-dependent kinases: cdk2 and cdk2L. Biochem. Biophys. Res. Commun. 197, 1524–1529.

Page, J., Suja, J.A., Santos, J.L., Rufas, J.S., 1998. Squash procedure for protein immunolocalization in meiotic cells. Chromosome Res. 6, 639–642.

Peters, A.H., Plug, A.W., van Vugt, M.J., de Boer, P., 1997. A drying-down technique for the spreading of mammalian meiocytes from the male and female germline. Chromosome Res. 5, 66–68.

Phillips, C.M., Dernburg, A.F., 2006. A family of zinc-finger proteins is required for chromosome-specific pairing and synapsis during meiosis in C. elegans. Dev. Cell. 11, 817–829.

Phillips, C.M., Wong, C., Bhalla, N., Carlton, P.M., Weiser, P., Meneely, P.M., Dernburg, A.F., 2005. HIM-8 binds to the X chromosome pairing center and mediates chromosome-specific meiotic synapsis. Cell 123, 1051–1063.

Ravnik, S.E., Wolgemuth, D.J., 1999. Regulation of meiosis during mammalian spermatogenesis: the A-type cyclins and their associated cyclin-dependent kinases are differentially expressed in the germ-cell lineage. Dev. Biol. 207, 408–418.

Scherthan, H., 2001. A bouquet makes ends meet. Nat. Rev. Mol. Cell Biol. 2, 621–627.

Scherthan, H., 2006. Factors directing telomere dynamics in synaptic meiosis. Biochem. Soc. Trans. 34, 550–553.

Scherthan, H., 2007. Telomere attachment and clustering during meiosis. Cell Mol. Life Sci. 64, 117–124.

Scherthan, H., Jerratsch, M., Li, B., Smith, S., Hulten, M., Lock, T., de Lange, T., 2000. Mammalian meiotic telomeres: protein composition and redistribution in relation to nuclear pores. Mol. Biol. Cell 11, 4189–4203.

Scherthan, H., Sfeir, A., de Lange, T., 2011. Rap1-independent telomere attachment and bouquet formation in mammalian meiosis. Chromosoma 120, 151–157.

Schmitt, J., Benavente, R., Hodzic, D., Hoog, C., Stewart, C.L., Alsheimer, M., 2007. Transmembrane protein Sun2 is involved in tethering mammalian meiotic telomeres to the nuclear envelope. Proc. Natl. Acad. Sci. USA 104, 7426–7431.

Sfeir, A., Kabir, S., van Overbeek, M., Celli, G.B., de Lange, T., 2010. Loss of Rap1 induces telomere recombination in the absence of NHEJ or a DNA damage signal. Science 327, 1657–1661.

Song, G., Wang, T., Guo, J., Lei, J., Li, C., Zheng, Z., Zhao, W., 2011. Identification of compatibility between ooplasmic factor and sperm gene in the intersubspecific crosses involving DDK and PWK mice strains. J. Genet. Genomics 38, 525–531.

Starr, D.A., Han, M., 2002. Role of ANC-1 in tethering nuclei to the actin cytoskeleton. Science 298, 406–409.

Starr, D.A., Hermann, G.J., Malone, C.J., Fixsen, W., Priess, J.R., Horvitz, H.R., Han, M., 2001. unc-83 encodes a novel component of the nuclear envelope and is essential for proper nuclear migration. Development 128, 5039–5050.

Sweeney, C., Murphy, M., Kubelka, M., Ravnik, S.E., Hawkins, C.F., Wolgemuth, D.J., Carrington, M., 1996. A distinct cyclin A is expressed in germ cells in the mouse. Development 122, 53–64.

Trelles-Sticken, E., Dresser, M.E., Scherthan, H., 2000. Meiotic telomere protein Ndj1p is required for meiosis-specific telomere distribution, bouquet formation and efficient homologue pairing. J. Cell Biol. 151, 95–106.

Ukomadu, C., Dutta, A., 2003. Inhibition of cdk2 activating phosphorylation by mevastatin. J. Biol. Chem. 278, 4840–4846.

Viera, A., Rufas, J.S., Martinez, I., Barbero, J.L., Ortega, S., Suja, J.A., 2009. CDK2 is required for proper homologous pairing, recombination and sex-body formation during male mouse meiosis. J. Cell Sci. 122, 2149–2159.

Ward, J.O., Reinholdt, L.G., Motley, W.W., Niswander, L.M., Deacon, D.C., Griffin, L.B., Langlais, K.K., Backus, V.L., Schimenti, K.J., O'Brien, M.J., Eppig, J.J., Schimenti, J. C., 2007. Mutation in mouse hei10, an e3 ubiquitin ligase, disrupts meiotic crossing over. PLoS Genet. 3, e139.